NEW LIMITS ON EARLY DARK ENERGY FROM THE SOUTH POLE TELESCOPE

C. L. Reichardt,[1] R. de Putter,[2,3] O. Zahn,[4] and Z. Hou[5]

Draft version January 12, 2012

ABSTRACT

We present new limits on early dark energy (EDE) from the cosmic microwave background (CMB) using data from the WMAP satellite on large angular scales and South Pole Telescope (SPT) on small angular scales. We find a strong upper limit on the EDE density of $\Omega_e < 0.018$ at 95% confidence, a factor of three improvement over WMAP data alone. We show that adding lower-redshift probes of the expansion rate to the CMB data improves constraints on the dark energy equation of state, but not the EDE density. We also explain how small-scale CMB temperature anisotropy constrains EDE.

Subject headings: dark energy — cosmic background radiation — early universe

1. INTRODUCTION

The mystery of cosmic acceleration is one of the most pressing questions in cosmology. We have strong evidence that the expansion of the Universe is accelerating from observations of supernovae (SNe – Perlmutter et al. (1999); Riess et al. (1998); Amanullah et al. (2010)), the cosmic microwave background (CMB – Komatsu et al. (2011); Das et al. (2011b); Keisler et al. (2011)) and galaxy surveys (Reid et al. (2010); Blake et al. (2011)). The simplest model for this acceleration is a cosmological constant. However, a wide range of alternative explanations exist, from modifications to general relativity to scalar fields.

To explain the observed cosmic acceleration, the dark energy (DE) equation of state (e.o.s.) must be close to $w = -1$ at late times. If w is constant, as for a cosmological constant and certain quintessence models, DE quickly becomes irrelevant as one looks back in cosmic history (the cosmological constant would be $\sim 10^{-9}$ of the total density at the time of CMB last scattering). In early dark energy (EDE) models, the e.o.s. was instead much larger in the past so that the DE density was considerable even in the early universe.

The best motivated EDE theories are so called "tracker" models (e.g. Ratra & Peebles (1988); Peebles & Ratra (1988); Wetterich (1988); Hebecker & Wetterich (2001)), which help to ameliorate the coincidence problem. While in non-early dynamical DE models the initial conditions must be very finely tuned in order for the DE density to be of the same order of magnitude as the matter density today, tracker models contain attractor solutions on which the DE evolution is determined by the e.o.s. of the dominant component of the universe, i.e. matter or radiation. The advantages are that the DE density can stay much closer to the energy density of the dominant component and that the DE evolution is independent of initial conditions. Tracer models, a subclass of tracker models, further limit the DE e.o.s. to be equal to the background e.o.s. so that $w = 1/3$ during radiation domination and $w = 0$ during matter domination. While the EDE fraction in generic tracker models is typically still quite small (although larger than in the constant w case), in tracer models it can easily be at the several percent level.

Several groups have used observations of the CMB, baryon acoustic oscillations (BAO), SNe, Ly-α forest and Hubble constant to constrain EDE models (Doran & Robbers 2006; Xia & Viel 2009; Alam et al. 2011; Calabrese et al. 2011). Current observations show no preference for a non-zero EDE density. The best upper limit on the EDE density from the CMB today is by Calabrese et al. (2011). Using large and small angular scale CMB observations from the WMAP7, ACBAR, QUaD and ACT experiments (Komatsu et al. 2011; Reichardt et al. 2009; Gupta et al. 2010; Das et al. 2011b), they find a 95% confidence upper limit on the EDE density of $\Omega_e < 0.043$ for a "relativistic" EDE model and $\Omega_e < 0.024$ for a "quintessence" model. As demonstrated by Xia & Viel (2009), adding high redshift measures of the growth factors and matter power spectrum can lead to much tighter (if potentially modeling dependent) constraints on EDE.

In this work, we present EDE constraints derived from the latest measurements of small-scale CMB anisotropy. We use bandpowers from the South Pole Telescope (SPT) (Keisler et al. 2011, hereafter K11), which are the best measurement of the CMB across the third to ninth acoustic peaks. We combine the SPT bandpowers with the WMAP7 bandpowers on larger angular scales in order to significantly tighten upper limits on the allowed EDE density. We also consider the effect of adding BAO and SNe data.

We present the EDE model in §2, and detail how EDE affects small-scale CMB anisotropy in §3. We describe the data we use in §4. Results are presented in §5, and we conclude in §6.

2. EDE MODEL

Instead of considering a specific model, we choose to constrain EDE in the more general tracer model parametrization by Doran & Robbers (2006). This

cr@bolo.berkeley.edu

[1] Department of Physics, University of California, Berkeley, CA USA 94720

[2] IFIC, Universidad de Valencia-CSIC, 46071, Valencia, Spain

[3] ICC, University of Barcelona (IEEC-UB), Marti i Franques 1, Barcelona 08028, Spain

[4] Berkeley Center for Cosmological Physics, Department of Physics, University of California, and Lawrence Berkeley National Labs, Berkeley, CA, USA 94720

[5] Department of Physics, University of California, Davis, CA, USA 95616

parametrization introduces two new parameters on top of the ΛCDM set, the DE e.o.s. at $z = 0$, w_0, and the DE density relative to the critical density at early times, Ω_e, which is taken to be constant at sufficiently high redshift ($z \gtrsim 10$). The DE density and e.o.s. are then given by

$$\Omega_{\mathrm{de}}(a) = \frac{\Omega_{\mathrm{de}}^0 - \Omega_e \left(1 - a^{-3w_0}\right)}{\Omega_{\mathrm{de}}^0 + \Omega_m^0 a^{3w_0}} + \Omega_e \left(1 - a^{-3w_0}\right) \quad (1)$$

$$w(a) = -\frac{1}{3[1 - \Omega_{\mathrm{de}}(a)]} \frac{d \ln \Omega_{\mathrm{de}}(a)}{d \ln a} + \frac{a_{eq}}{3(a + a_{eq})}. \quad (2)$$

Here a_{eq} is the scale factor at matter-radiation equality, and Ω_{de}^0 (Ω_m^0) is the DE (matter) density relative to critical density at $z = 0$. This parametrization assumes spatial flatness so that $\Omega_m^0 + \Omega_{\mathrm{de}}^0 = 1$. Since we force $\Omega_{\mathrm{de}}(a)$ to be constant at high redshift, the DE e.o.s. mimics that of the dominant component at early times, thus behaving like a tracer model. Later during matter domination, at $z < 10$, the e.o.s. transitions towards its current value, w_0, so it can account for cosmic acceleration.

To consistently describe the perturbations, we are motivated by quintessence models to treat DE as a perfect fluid with a sound speed, c_s, equal to the speed of light (see Hu (1998)). This choice together with the parametrization for the background evolution completely specifies the behavior of DE. We only consider models with $w_0 \geq -1$ and thus do not entertain the possibility of "phantom crossing" (see e.g. Fang et al. (2008)). This restriction allows us to avoid pathologies in perturbation evolution and to stay in the quintessence regime.

3. HOW THE CMB CONSTRAINS EDE

EDE directly influences the evolution of acoustic oscillations, and thus imprints a much stronger signature on the CMB temperature anisotropy than late-time DE. In contrast, late-time DE only affects the CMB through its effect on the distance to last scattering and the integrated Sachs Wolfe (ISW) effect, leading to a strong degeneracy between DE parameters with CMB data alone.

First of all, EDE increases the expansion rate, rescaling the Hubble parameter at high redshift by a constant factor $H \rightarrow (1 - \Omega_e)^{-\frac{1}{2}} H$. Since quintessence-like (with $c_s = 1$, the speed of light) DE does not cluster on scales smaller than the horizon, the result is a suppression of the growth of cold dark matter and metric perturbations after matter radiation equality. This suppression in turn drives a boost in the amplitude of oscillations in the baryon-photon plasma.

The effect of adding EDE is similar to the better known effect of increasing the radiation to matter ratio (see e.g. Hu et al. (1997)). Indeed, Calabrese et al. (2011) show that EDE can be related to a time-dependent effective number of relativistic species, ΔN_{eff}, which is roughly four times higher at recombination than during big-bang nucleosynthesis (BBN). Temperature modes entering during radiation domination ($\ell > \ell_{eq}$) when the growth of metric perturbations is suppressed, undergo a boost relative to those entering during matter domination ($\ell < \ell_{eq}$). Increasing the radiation to matter ratio shifts ℓ_{eq} to lower values, thereby enhancing the amplitude at ℓ near ℓ_{eq}.

Analogously, Ω_e shifts the scale corresponding to the time of equality between clustering matter and non-clustering radiation & DE according to $\ell_{eq} \rightarrow \sqrt{1 - 2\Omega_e}\, \ell_{eq}$ (since the distance to the CMB last scattering surface also decreases with increasing Ω_e, EDE causes the angular mode ℓ_{eq} to shift to a smaller value). However, the exact signature of the boost has a different scale dependence than the effect due to simply changing the relative amounts of matter and radiation (for example by varying the effective number of relativistic species, N_{eff}) because, after radiation domination, the DE density does not decay as fast as that of radiation.

In addition to boosting the acoustic oscillations, the increase in the Hubble scale due to EDE changes the sound horizon scale at decoupling, the Silk damping scale and the distance to last scattering. Finally, the lack of clustering in the DE contributes to the early ISW effect, and hence increases power for modes larger than the first acoustic peak.

While the signatures discussed above are to a degree degenerate with variations in other cosmological parameters, there remains a clear EDE signature even after taking this into account, as shown in Fig. 1. Here, for values of Ω_e spaced in 0.01 increments from $\Omega_e = 0$ to 0.05, we show the best-fit WMAP7 (Larson et al. 2011) spectrum. Clearly, after accounting for parameter degeneracies with the large-scale CMB data, there is a strong signature of EDE on small scales ($\ell > 1000$). Increasing the EDE density increases the small scale power because it shortens the Silk damping length at the last scattering surface. The angular diameter distance decreases to a lesser degree; somewhat reducing the net change to the angular size of Silk damping. The physical sound horizon and angular diameter distance are reduced by similar amounts so the positions of the acoustic peaks move only slightly to larger scales. The reduced damping further reduces the apparent shift in position of the first peaks. The clear signal at $\ell > 1000$ strongly motivates using the SPT power spectrum measurement by K11, as it provides the best measurement to date of the CMB temperature anisotropy over the Silk damping tail.

EDE also affects the BBN helium prediction; however this effect does not contribute significantly to the current CMB constraints. With respect to BBN, EDE is equivalent to adding (non-interacting) relativistic species, $\Delta N_{\mathrm{eff}} \sim 7.44\Omega_e$, which affect the helium fraction through $\Delta Y_{\mathrm{He}} \sim 0.013 \Delta N_{\mathrm{eff}}$ (Calabrese et al. 2011). Even $\Omega_e = 0.05$ (the $2\,\sigma$ limit from WMAP7 only) would change the helium fraction by only $\Delta Y_{\mathrm{He}} \sim 0.005$, which is small compared to the WMAP7+SPT Y_{He} uncertainty of 0.03 (K11). The impact of EDE on the helium abundance is therefore negligible for the CMB constraints.

There are clear reasons to concentrate on the CMB anisotropy when considering EDE theories. Given that we have implemented a generalized tracer model for the EDE, the model mimics normal DE in the current, DE-dominated epoch. The effect of Ω_e at late times is similar to having a varying e.o.s. $w_a \approx 5\Omega_e$ (Linder & Robbers (2008)) and is thus very weak. Therefore, observations of the low-redshift universe, such as SNe, BAO, and CMB lensing, primarily constrain Ω_{de}^0 and w_0.

4. DATA

This work focuses on how small-scale CMB data complement large-scale CMB data to constrain EDE. Therefore we include large-scale CMB bandpowers from the
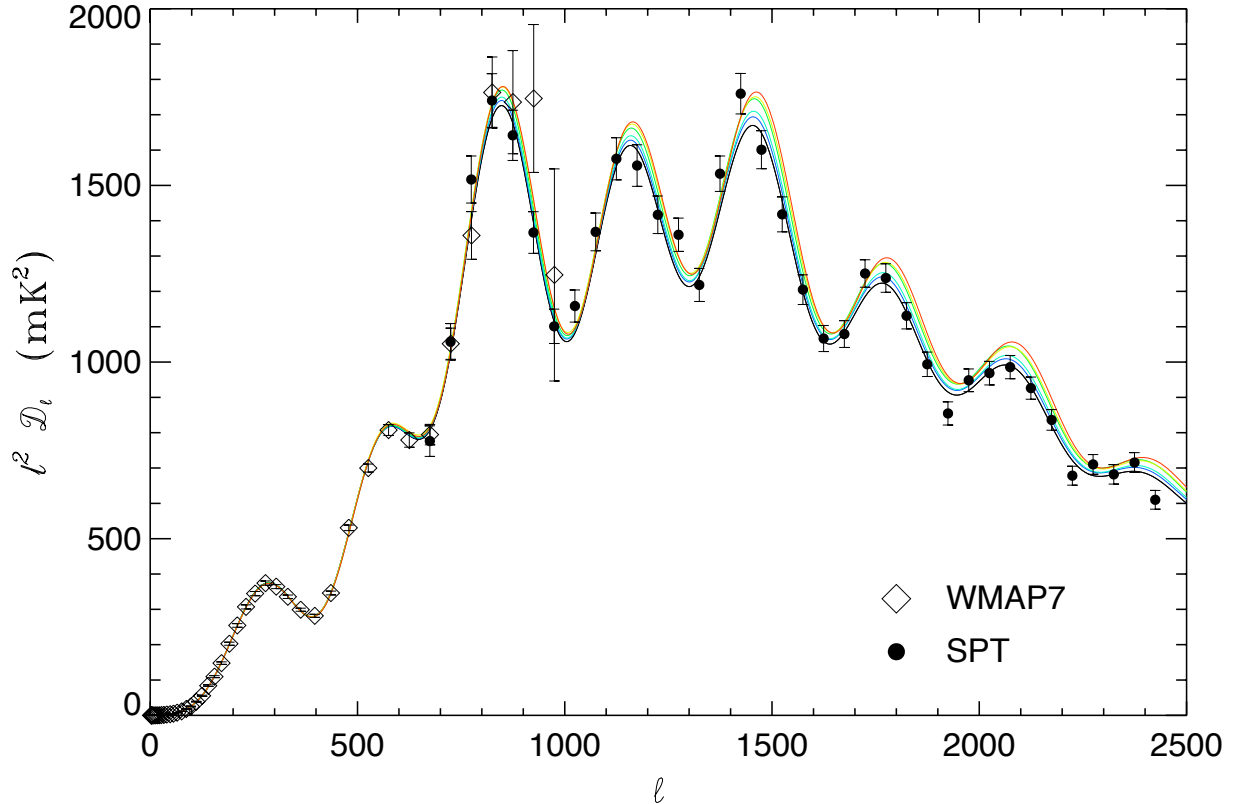
Fig. 1.— The WMAP7 bandpowers over-plotted on the best-fit WMAP7 model as Ω_e varies from 0 (black) to 0.05 (red). All the models can accommodate the WMAP7 bandpowers at low ℓ. However, models with more EDE predict more power at higher ℓ (smaller angular scales). Measuring the CMB power spectrum on small angular scales with experiments such as SPT (and *Planck* in the future) can thereby strengthen the limits on EDE. We include the SPT bandpowers in the plot to illustrate their constraining power.

seven-year WMAP data release (WMAP7, Larson et al. 2011) in all parameter chains. The best current constraints on small-scale CMB power spectrum come from an analysis of $800 \deg^2$ of sky observed with the SPT (K11). The K11 bandpowers cover angular multipoles from $500 < \ell < 3000$. The covariance between the WMAP and K11 bandpowers is negligible (K11). However, it is non-trivial to combine the K11 bandpowers with those from other experiments focused on the CMB damping tail (e.g. Reichardt et al. (2009); Das et al. (2011a)) since the experiments are cosmic variance limited and have overlapping sky coverage. Hence we restrict ourselves to the K11 bandpowers to constrain the small-scale CMB temperature anisotropy.

We also consider EDE constraints from geometrical observations at lower redshift. Specifically, we look at three additional datasets: BAO observations, Hubble constant data (referred to as 'H_0'), and SNe data. We use observations from SDSS and 2dFGRS of the BAO feature (Percival et al. 2010). Percival et al. (2010) use the BAO feature to measure the angular diameter distance relation. We also use direct, low-redshift measurements of the Hubble constant with the Hubble Space Telescope that found $H_0 = 73.8 \pm 2.4 \, \mathrm{km \, s^{-1} \, Mpc^{-1}}$ (Riess et al. 2011). For SNe, we add the Supernovae Cosmology Project's Union2 dataset (Amanullah et al. 2010) which constrains the luminosity distance-redshift relation.

5. RESULTS

We fit the data to a model for the lensed primary CMB anisotropy. Parameter constraints are calculated using the publicly available CosmoMC[6] package (Lewis & Bridle 2002). The CMB power spectrum for a given cosmology is calculated using the CAMB[7] package (Lewis et al. 2000). We have modified both packages to include the EDE prescription outlined in §2. This model has eight free parameters: $\Omega_b h^2$, $\Omega_c h^2$, A_s, n_s, τ, Ω_{de}^0, w_0 and Ω_e. We do not consider additional cosmological parameters such as the neutrino energy density fraction or N_{eff}, but note that Joudaki & Kaplinghat (2011) and Calabrese et al. (2011) suggest that Ω_e is largely independent of these parameters. We also include in all parameter chains the three nuisance foreground terms described by K11; these nuisance terms negate the information from the amplitude (but not peak structure) of the power spectrum at $\ell \gtrsim 2500$. We have made one change to the foreground terms; we have changed the template shape of the clustered component of the cosmic infrared background to a pure power law ($D_\ell \propto \ell^{0.8}$) to reflect recent constraints from SPT, ACT, Planck, and BLAST (Reichardt et al. 2011; Addison et al. 2011). The Monte Carlo Markov chains are available for download at the SPT website.[8]

We consider the eight data combinations described in §4. The resulting constraints on DE are summarized in

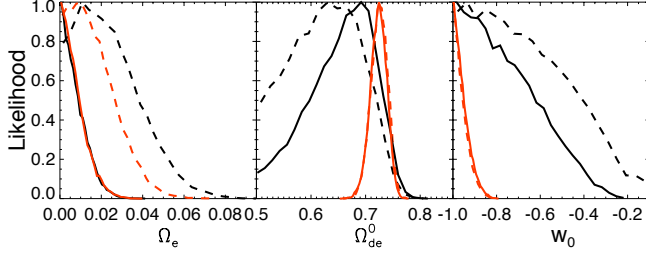FIG. 2.— Posterior probabilities for Ω_e (**Left panel**), Ω_{de}^0 (**Middle panel**), and w_0 (**Right panel**). **Black lines** show constraints from the CMB alone. **Red lines** show constraints from the CMB + BAO + H_0 + SNe. **Solid lines** include the SPT bandpowers from K11 in addition to WMAP7; **dashed lines** include only WMAP7 data.

Table 1 and plotted in Figure 2. With only the large-scale CMB observations from WMAP, the geometrical measures tighten the upper limit on EDE by 30% from $\Omega_e < 0.052$ to $\Omega_e < 0.037$ at 95% CL. This improvement results from better measurements of $\Omega_m h^2$, n_s and Θ_s, which are somewhat degenerate with Ω_e. Notably however, as expected from §3, the EDE constraints are completely determined by the CMB power spectrum once the spectrum is measured over the Silk damping tail. The small-scale CMB bandpowers tighten the upper limit by a factor of three over the large-scale CMB data alone to $\Omega_e < 0.018$. The 95% confidence upper limit on Ω_e remains unchanged at ~ 0.018 when BAO, H_0 and SNe observations are added to the CMB power spectrum.

Conversely, the geometrical constraints are essential for the local (z=0) DE parameters. Both the current DE density and its e.o.s. are poorly constrained by the CMB alone, as shown in Table 1 and Figure 2.

We show the main degeneracies in the CMB data between the EDE density and other parameters in Figure 3. The red, orange and yellow filled contours denote the $68.3, 95.4$ and 99.7% CL regions with WMAP7 data. The solid black lines mark the same likelihood regions for WMAP7 + SPT data. We do not see a strong degeneracy between the EDE density and either late time DE parameter (w_0 or Ω_{de}^0). The w_0-Ω_e plane is shown in the top right panel. We do see degeneracies in the WMAP7 constraints between Ω_e and $\Omega_m h^2$, Θ_s, and n_s, shown in the top left, bottom left and bottom right panels respectively. Perhaps unsurprisingly given the importance of the high-ℓ bandpowers to measuring EDE, these are also the three parameters for which adding small-scale CMB data has the largest impact (K11). The strongest degeneracy is between Ω_e and the angular scale of the acoustic peaks, Θ_s. This is the ΛCDM parameter best constrained by the SPT data since the SPT bandpowers improve measurements of the third to ninth acoustic peaks. The SPT bandpowers also improve the WMAP7 constraints on n_s by 30% and on $\Omega_m h^2$ by 15%. The $\Omega_m h^2$ is coming primarily from the third acoustic peak, while the n_s constraint comes from extending the range of angular scales probed. For all three parameters, the SPT bandpowers reduce the degeneracies with Ω_e. As shown in Figure 3, the allowed regions of the parameter planes are reduced by much more than the 15-30% numbers mentioned above.

The effect of EDE on observables depends on its clustering properties. As discussed in section 2, inspired by quintessence models, the best motivated approach
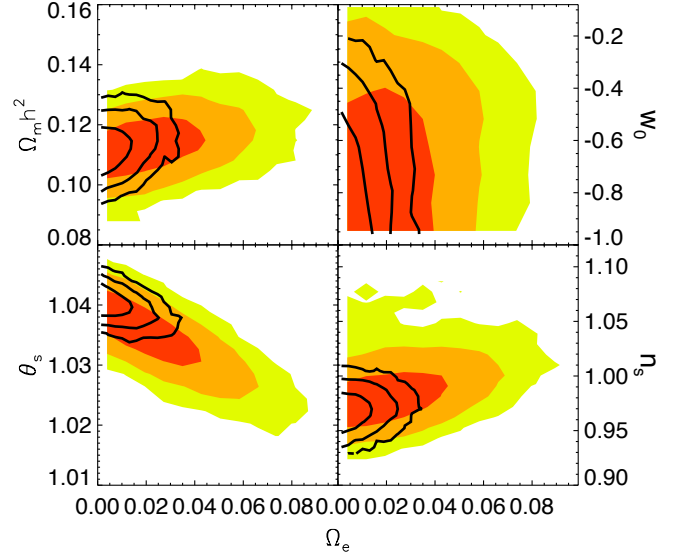

FIG. 3.— 2D likelihood surfaces between Ω_e and the three most correlated parameters: $\Omega_m h^2$ (*top left panel*), Θ_s (*bottom left panel*), and n_s (*bottom right panel*). We also show the likelihood surface for Ω_e and the DE e.o.s. at $z = 0$, w_0 (*top right panel*). Ω_e is largely independent of the remaining parameters (Ω_{de}^0, A_s, τ and $\Omega_b h^2$). Contours mark the $68.3, 95.4$ and 99.7% confidence regions. The **filled, colored contours** show the constraints from WMAP7 data only. The **black line contours** show the constraints when the SPT small-scale CMB bandpowers are added.

is to treat the DE as a perfect fluid with rest frame sound speed $c_s = 1$. However, more exotic models such as k-essence (Armendariz-Picon et al. (2000); Chiba et al. (2000)) can have sound speeds below the speed of light and thus allow significant DE perturbations on sub-horizon scales. To illustrate how the EDE bound depends on assumptions about DE perturbations, we briefly consider two alternative models with $c_s = 0$ or $1/\sqrt{3}$. In the $c_s = 0$ case, DE is free to cluster on all scales, and in this particular sense it behaves more like cold dark matter, although the DE perturbations receive the usual suppression when the e.o.s. $w \to -1$ at late times (e.g., de Putter et al. (2010)). Our default $c_s = 1$ case is more similar to radiation where perturbation growth is suppressed by pressure perturbations. We also look at $c_s = 1/\sqrt{3}$ since it leads to weakest constraints on Ω_e.

In the $c_s = 0$ case, the WMAP7 upper limit on the EDE density is $\Omega_e < 0.049$, nearly unchanged from the baseline $c_s = 1$ case. However, the limits weaken for the other data sets. The 95% upper limit strengthens to $\Omega_e < 0.035$ with WMAP7 + K11, and remains nearly unchanged for the maximal data set WMAP7 + K11+ BAO + H_0 +SNe. These limits are a factor of two weaker than in the baseline case.

Looking at the c_s-Ω_e plane, we find the weakest constraints on Ω_e at $c_s^2 = 1/3$. For WMAP7 only, the 95% upper limit is $\Omega_e < 0.119$, a factor of two higher than for $c_s^2 = 1$. Adding BAO + H_0 +SNe or K11 data improves the limit by a factor of 1.6. Adding all of these reduces the 95% upper limit to $\Omega_e < 0.055$, a factor of three higher than for $c_s^2 = 1$.

6. CONCLUSION

We find an upper limit on the EDE density of $\Omega_e < 0.018$ from CMB data alone. We show that the SPT data

TABLE 1
Dark energy constraints

Ω_e	CMB	CMB + BAO + H$_0$	CMB + SNe	CMB + BAO + H$_0$ +SNe
WMAP7 only	< 0.052	< 0.038	< 0.039	< 0.037
WMAP7+SPT	< 0.018	< 0.018	< 0.018	< 0.019
Ω_{de}^0				
WMAP7 only	0.608 ± 0.093	0.720 ± 0.018	0.716 ± 0.025	0.726 ± 0.016
WMAP7+SPT	0.660 ± 0.067	0.720 ± 0.017	0.722 ± 0.023	0.724 ± 0.015
w_0				
WMAP7 only	< −0.29	< −0.84	< −0.87	< −0.89
WMAP7+SPT	< −0.45	< −0.84	< −0.86	< −0.90

NOTE. — Constraints on the early and late-time ($z = 0$) DE densities, Ω_e and Ω_{de}^0, and e.o.s., w_0, for different datasets. We report 95% confidence upper limits on the EDE density and DE e.o.s.. The priors on these parameters require that they be greater than 0 and -1 respectively. We report 1σ uncertainties on the $z = 0$ DE density, Ω_{de}^0. Geometrical constraints from BAO, H$_0$ and SNe are very important for the late-time DE parameters (w_0 and Ω_{de}^0). However, the constraint on the EDE density is primarily from the CMB temperature anisotropy.

make observations of the low redshift expansion history redundant, i.e. the CMB constraint is not improved further using BAO or SNe data. The constraining power comes from EDE's impact on the Universe's expansion rate at $z \sim 1100$. This leads to relatively more power at small angular scales and to small shifts in the peak positions. Small angular scale CMB observations of the higher acoustic peaks break degeneracies in the WMAP data between the EDE density and the position of the acoustic peaks, the matter density and slope of the primordial power spectrum. In the next year, we expect order of magnitude improvements in measurements of the small-angular scale CMB power spectrum from the SPT, ACT and especially *Planck* surveys. These experiments promise to further elucidate the properties of DE in the early Universe.

REFERENCES

Addison, G. E., et al. 2011, arXiv:1108.4614
Alam, U., Lukić, Z., & Bhattacharya, S. 2011, ApJ, 727, 87
Amanullah, R., et al. 2010, ApJ, 716, 712
Armendariz-Picon, C., Mukhanov, V., & Steinhardt, P. J. 2000, Physical Review Letters, 85, 4438
Blake, C., Kazin, E. A., Beutler, F., et al. 2011, MNRAS, 418, 1707
Calabrese, E., Huterer, D., Linder, E. V., Melchiorri, A., & Pagano, L. 2011, Phys. Rev. D, 83, 123504
Chiba, T., Okabe, T., & Yamaguchi, M. 2000, Phys. Rev. D, 62, 023511
Das, S., et al. 2011a, Physical Review Letters, 107, 021301
—. 2011b, ApJ, 729, 62
de Putter, R., Huterer, D., & Linder, E. V. 2010, Phys. Rev. D, 81, 103513
Doran, M., & Robbers, G. 2006, JCAP, 6, 26
Fang, W., Hu, W., & Lewis, A. 2008, Phys. Rev. D, 78, 087303
Gupta, S., et al. 2010, ApJ, 716, 1040
Hebecker, A., & Wetterich, C. 2001, Physics Letters B, 497, 281
Hu, W. 1998, Astrophys. J., 506, 485
Hu, W., Sugiyama, N., & Silk, J. 1997, Nature, 386, 37

Joudaki, S., & Kaplinghat, M. 2011, arXiv:1106.0299
Keisler, R., et al. 2011, ApJ, 743, 28
Komatsu, E., et al. 2011, ApJS, 192, 18
Larson, D., et al. 2011, ApJS, 192, 16
Lewis, A., & Bridle, S. 2002, Phys. Rev. D, 66, 103511
Lewis, A., Challinor, A., & Lasenby, A. 2000, ApJ, 538, 473
Linder, E. V., & Robbers, G. 2008, JCAP, 6, 4
Peebles, P. J. E., & Ratra, B. 1988, ApJ, 325, L17
Percival, W. J., et al. 2010, MNRAS, 401, 2148
Perlmutter, S., et al. 1999, ApJ, 517, 565
Ratra, B., & Peebles, P. J. E. 1988, Phys.Rev.D, 37, 3406
Reichardt, C. L., et al. 2009, ApJ, 694, 1200
—. 2011, arXiv:1111.0932
Reid, B. A., et al. 2010, MNRAS, 404, 60
Riess, A. G., et al. 1998, AJ, 116, 1009
Riess, A. G., et al. 2011, ApJ, 730, 119
Wetterich, C. 1988, Nuclear Physics B, 302, 668
Xia, J.-Q., & Viel, M. 2009, JCAP, 4, 2